Tomographic wire-grid imaging of magnetic surfaces

B. D. Blackwell, J. Howard, and R. B. Tumlos
Plasma Research Laboratory, Research School of Physical Sciences and Engineering, The Australian National University, Canberra, Australia

(Presented on 17 March 1992)

We describe a new, fast, and accurate method for obtaining magnetic surface puncture plots by the use of a rotating grid of fine wires. Electrons launched from a small gun follow the magnetic field lines, and a fraction are intercepted by the wire grid. The current signals, chordal integrals of electron beam intensity, are inverted by an iterative pseudotomographic method to obtain an image of the electron beam density in the plane of the grid, that is, a puncture plot of the magnetic surface. The method is capable of high resolution while maintaining a high transparency to electrons, and is demonstrated on a small toroidal stellarator, the SHEILA heliac.

I. INTRODUCTION

The complex magnetic geometry of plasma confinement devices is crucial to their successful operation, and must be verified by direct measurement. This can be achieved by mapping the trajectories of electrons launched along magnetic field lines inside the confinement volume. A fast acquisition time ($\ll$1 h) is important during commissioning to facilitate the optimization of coil positions, and to assess a large number of possible sources of error. Once operational, the large number of adjustable parameters of flexible confinement devices requires routine mapping of the resulting wide range of magnetic configurations.

Three techniques are currently in use—direct collection by point probes,[1] optical imaging of fluorescent emissions of electrons striking a highly transparent coated mesh grid,[2] or a fluorescent coated rod swept slowly across the surface.[3] The first method requires a two-dimensional scan for each surface and is tedious. The mesh technique obtains a complete surface in one measurement, but is limited in resolution to the mesh spacing, which is in turn restricted by transparency requirements. The fluorescent rod method overcomes the resolution problem, and produces magnetic field maps of high quality.[4] A modification[5] to include inbuilt image intensification allows reduction of electron velocities ($\leqslant$10 eV) so that measurements free of curvature drift errors can be performed at low magnetic fields ($\simeq$0.1 T) typical of continuous operation of pulsed plasma devices.

In the technique described here, the electrons are intercepted and collected by a grid of tautly stretched, parallel fine wires which can be rotated in small steps to scan the cross section, and the image is obtained by pseudotomographic inversion. The method has the advantage of sensitivity to low-energy electrons (minimum drift) and the grid detector can be simply constructed to any desired size and resolution. The rotational motion of the grid is inherently accurate and controllable, allows consistency checks based on symmetries, and avoids the need to correct the image distortion of optical viewing.[5] The proof-of-principle apparatus described here was constructed for the SHEILA prototype heliac[6] (Fig. 1, R/a=0.19/0.03 m, $B_0 \leqslant 0.2$ T and $0.6 < \iota < 2$) in preparation for installation of a more sophisticated detector on the larger machine H-1.[7]

II. APPARATUS

The prototype grid consists of 11×0.3-mm molybdenum wires spaced over 35 mm stretched in a circular insulating frame (78 mmϕ) and tensioned by adjusting screws (Fig. 2). One mechanical complication for a machine with a central ring conductor (e.g., heliac) is that the frame supporting the wires may have to link the ring. For this prototype detector, however, the frame does not link the ring conductor, allowing simple installation and removal for calibration, adjustment, and modification, but because of mechanical obstruction by the smaller frame, only the interior magnetic surfaces are accessible.

A threaded rod supported by a simple o-ring feedthrough provides the angular drive for the prototype grid. The grid frame is shielded on one side, and is fitted into a

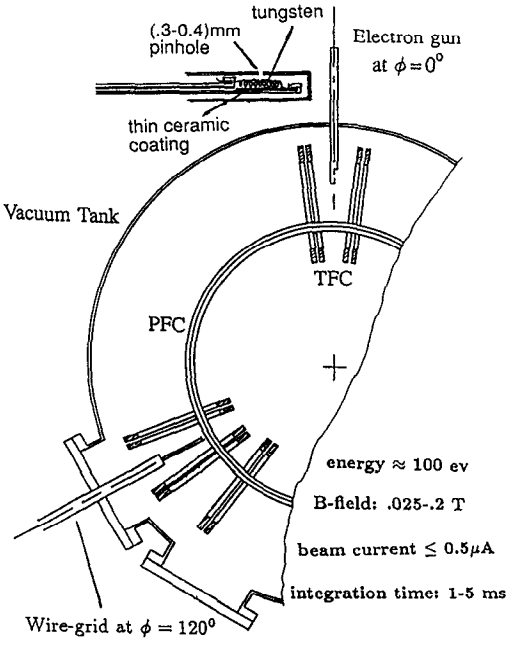

FIG. 1. The top view of the electron beam experiment in SHEILA showing some toroidal field coils (TFC), the ring conductor (PFC), the wire grid, and the 2.5-mm electron gun (inset).

 0034-6748/92/104725-03$02.00

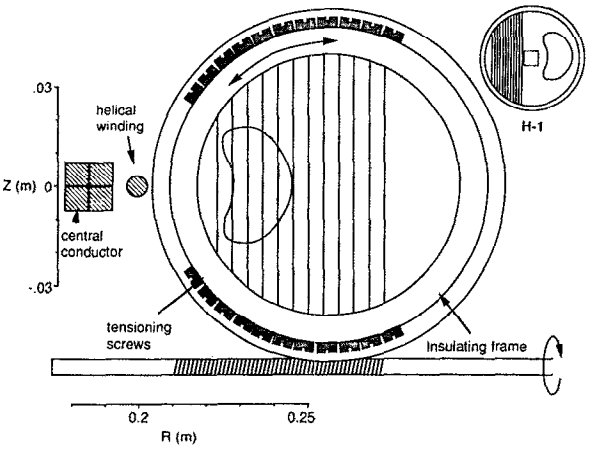

FIG. 2. Wire grid at $\theta=0$ (inset: proposed H-1 grid).

brass ring on the other side which houses the angular drive rod and provides further shielding and support. An important function of the shielding is to prevent electron pickup by the tensioning screws and connections, which may otherwise collect significant currents. Electrons are launched from a diode gun at energies of 100 eV with ~ 1-μA beam current.

Current signals into an effective resistance of 125 kΩ are passed through a 300-Hz low-pass 4-pole Bessel filter into a 12-bit digitizer. Eleven channels of chordal current data are recorded and analyzed using MDS (MIT, Cambridge, MA) and IDL (Research Systems, Inc., Boulder, CO) acquisition and analysis software. Although the final system will scan through all angles in a few tens of seconds, limitations of the SHEILA heliac required the data for this experiment to be acquired one shot at a time, at 30-s intervals.

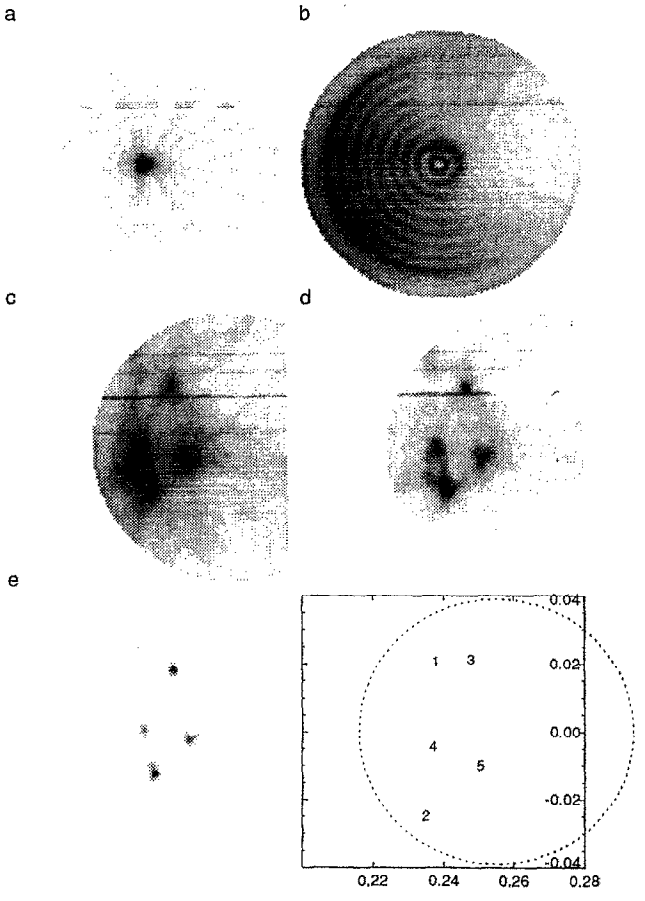

FIG. 3. Reconstructed images (a) a typical point spread function, (b) the instrument function, (c) data from Fig. 4 after 1, 2(d) and 6(e) iterations, and (f) the punctures computed from measured coil currents. Images c, d, and e have been divided by image b.

III. ANALYSIS

The nature of the data and the requirements of the reconstruction process differ from other applications of tomography. The data gathering technique is slightly perturbative: current detected in the first transit reduces the signal for subsequent transits, and the perturbation changes with grid position. Further perturbation may occur if the beam is slightly deflected or scattered by the grid. The small number of wires desirable for transparency causes undersampling which can only be partly compensated by oversampling in angle. This is illustrated by the point-spread function [Fig. 3(a)], in which the $1/r$ decay quickly breaks up into a number of spokes, determined by the smaller of the number of views and wires. Because of the lack of self-consistency between projections and this sparse sampling, standard tomographic methods give noisy, alias-contaminated, and poorly resolved images.[8]

From the many measurements, however, it is required to determine only the location of a small number of delta-function-like electron beam punctures. The low information content and the nature of the image suggests that a hybrid tomographic/coincidence method that favors *a priori* the point-like structure of the image can be used for extraction of the punctures. For unbiased and accurate reconstructions, there should be a uniform and high density of wire intersections (sampling density) in the image plane. The sampling density illustrated in Fig. 3(b) tends to have an annular structure with peaks where the wires are tangent to their circular locii of rotation, and sampling is nonuniform near the center.

For both a quick initial analysis (<1 min, DECStation 5000) and as the first step of a more sophisticated iterative analysis, the chordal current signals can be simply back-projected with a Gaussian profile onto an array of (typically) 128×128 pixcells, summing contributions over all 11 wires and 140 angles ($[0..\pi]$). The choice of the width of the Gaussian is a compromise between resolution and the introduction of spurious features, and should be chosen to be near the larger of the wire spacing and the wire/electron beam diameter.

To refine the reconstruction, and to de-emphasize ghost points, the process was iterated by creating an image mask that is some function of the initial reconstruction, and redistributing the chordal currents by backprojecting according to the mask weight. Selection of parameters that

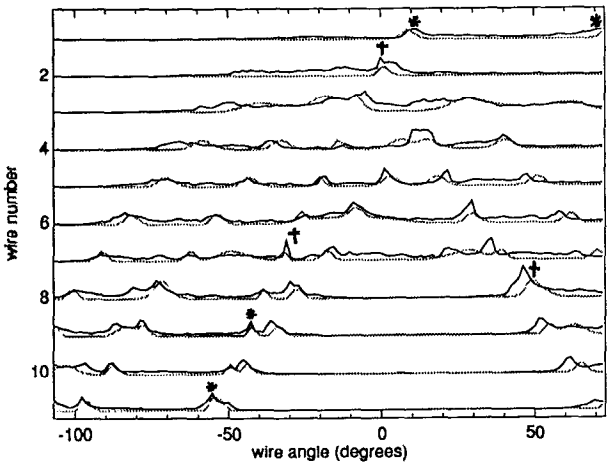

FIG. 4. Raw chordal current signals from a typical surface scan (*, † see text).

control the form of the mask is a balance between rapid convergence of successive iterations and the minimization of spurious points. Simulations for 11 wire/140 view experiments have shown that the puncture coordinates can be recovered to an accuracy of better than 2%.

Details of the numerical enhancement techniques cannot be fully treated here, but some observations can be made. The effect of attenuation has been numerically simulated both by deterministically accounting for beam losses according to how close the beam passes to a wire on each transit, and by multiplying simulated signals by different scale factors for each transit, randomly varying between 0.5 and 1.5. Accurate reconstructions were possible in both cases. In fact, variation in intensity of the recovered punctures indicates the sequence of electron transits and can be used to infer the rotational transform, if the data quality is good. The results presented here indicate a transparency of >0.7, to be compared with the geometrical transparency of $\simeq 0.9$.

IV. RESULTS

The collected wire currents are shown in Fig. 4 for a magnetic configuration chosen for simplicity comprising just 5 punctures ($\iota \simeq 8/5$). The signals are relatively clean and uniform across the wire array. The sharper peaks correspond to puncture points closer to the perimeter of the ring where the tangential scanning velocity is highest. Peaks marked *, representing the same point, were used for consistency checks.

The simple backprojected image obtained using these data shown in Fig. 3(c) is blurred by the $1/r$ behavior of the point spread function. Just one redistributing iteration [Fig. 3(d)] enhances the image and points are recovered after 10–30 iterations. The size and shape of the surface indicated by the five reconstructed image points conforms well with the magnetic surface computed using the measured coil currents. The displacement of the surface is a typical result of small error fields that motivate surface mapping. Further investigations are underway to determine the source of the error field. The equal spacing (in magnetic coordinates) of the 5 points indicates close proximity to a surface having rotational transform $\iota = N/5$, and other measurements show that $N=8$, indicating an error of less than 1% compared to the computer field-line tracing result of $\iota = 1.61$.

It is instructive to compare the expected current signals produced by an idealized reconstructed image with the measured wire currents. The shaded lines in Fig. 4, the projections of 5 points at the locations in Fig. 3(e) with Gaussian widths of 1 mm, reproduce all the significant features of the measured currents. The slight displacement of some features may be attributable to slight bowing of some wires with frame rotation. The widths of the features match well except for some fine structure in the data suggesting a sharp peak superimposed on a broader peak († in Fig. 4).

Time variation of signals during the rise and fall of the magnetic field was observed. This is attributed to configuration changes caused by small mismatches in the current waveforms on each magnetic field coil set, and more importantly by time-varying eddy currents in the thick top and bottom vacuum flanges (first detected using this technique). There is occasionally evidence for secondary emission from the wires in the form of negative nett current signals. This is more apparent at lower electron energies (<90 eV) but is expected to decrease at very low energies with the reduced secondary electron yield (impractical on SHEILA because of the unshielded coil potentials).

These first measurements under the challenging conditions of a small, pulsed, low magnetic field device verify the principle of the technique, and demonstrate high resolution relative to the small surface size. A full-sized, captive grid is proposed for H-1 (inset in Fig. 2). The grid has more wires(32), each tensioned by springs, and can be rotated 180° out of the confinement volume to allow plasma operation. Shielded coils in H-1 will allow the exploitation of very low energy beams ($\lesssim 30$ eV) and low secondary emission materials.

The authors are pleased to acknowledge the encouragement and support of S. M. Hamberger, and the technical assistance of E. Wedhorn, J. Wach, and R. Kimlin. Computer time on the Fujitsu VP2200 supercomputer was provided by the ANU Supercomputer Facility.

[1] R. M. Sinclair, J. C. Hosea, and G. V. Sheffield, Rev. Sci. Instrum. **41**, 1552 (1970).
[2] R. J. Colchin, F. S. B. Anderson, A. C. England, R. F. Gandy *et al.*, Rev. Sci. Instrum. **60**, 2680 (1989).
[3] H. Hailer, J. Massig, F. Schuler, K. Schworer, and H. Zwicker, 14th European Conf. on Controlled Fusion and Plasma Physics, Madrid, 1987.
[4] J. Sapper and H. Renner, Fusion Technol. **17**, 62 (1990).
[5] T. Y. Tou, B. D. Blackwell, and L. E. Sharp, Rev. Sci. Instrum. **62**, 1149 (1991).
[6] B. D. Blackwell, S. M. Hamberger, L. E. Sharp, and X-H Shi, Aust. J. Phys. **42**, 73 (1989).
[7] S. M. Hamberger, B. D. Blackwell, L. E. Sharp, and D. B. Shenton, Fusion Technol. **17**, 123 (1990).
[8] J. Howard, J. Opt. Soc. Am. A **5**, 999 (1988).